INTERNATIONAL JOURNAL OF ADVANCE RESEARCH, IDEAS AND INNOVATIONS IN TECHNOLOGY

ISSN: 2454-132X
Impact Factor: 6.078
(Volume 9, Issue 2 - V9I2-1338)
Available online at: https://www.ijariit.com

Maximum Power Point Tracking (MPPT) for a PV System Using a P&O Algorithm for Rapid and Accurate Response to Ambient Conditions

Yasir Rahman
engr.yasir804@gmail.com
University of Engineering and Technology Peshawar, Pakistan

Muhammad Iftikhar Khan
Muhammad Iftikhar Khan
University of Engineering and Technology Peshawar, Pakistan

Ihtisham ul Haq
ihtishamulhaq.eep@uetpeshawar.edu.pk
University of Engineering and Technology Peshawar, Pakistan

Mamoon Ur Rashid
mamoonurrashid196@gmail.com
CECOS University, Peshawar, Pakistan

Abstract

In order to maximize the efficiency of PV systems, this research proposes a new method of MPPT known as enhanced adaptive perturb and observe (EA-P&O). The objective is to address Issues with conventional P&O, such as its propensity for steady-state oscillation, its unreliable tracking, and its inability to spot the global peak when it is obscured in some way. To address the first two problems, we introduce a unique oscillation detection mechanism and a dynamic boundary condition. A sophisticated forecasting system is currently being created to monitor the worldwide peak on a continuous basis. The fact that open-circuit voltage can be determined without the inclusion of external sensors is still another perk. To ensure the concept is feasible, we run simulations in Matlab under rigorous dynamic irradiance and partial shading circumstances. Adding more experimental proof with the help of a buck-boost converter and a dSpace DS1104 DSP processor. The algorithm is compared to the artificial bee colony, modified incremental conduction, cuckoo search, and hybrid ant colony Optimization-P&O, all of which are well-known MPPT approaches. The results show that the suggested method succeeds where others fail when trying to follow the global peak in varying degrees of partial shade. Additionally, the tracking speed has been multiplied by three, while maintaining 99% accuracy.

Keywords: **MPPT, PV, Solar, tracking MPP, Optimization**

I. INTRODUCTION

There has been an uptick in the development of MPPT algorithms for solar systems, and many of these newer algorithms make use of soft computing methods. Differential evolution (DE) ANNs, particle swarm optimization, ant colony optimization, artificial bee colony, grey wolf firefly, cuckoo search, etc., are some of the more well-known methods used for maximum power point tracking (MPPT) recently. The techniques' greatest strength is in their ability to adapt readily to novel conditions.

Modifications made to the ambient lighting and shadows. Improved efficiency is outweighed by drawbacks such as complexity, processor strain, implementation expense, and sluggish tracking speed. In response, a slew of new articles have revisited and improved upon tried-and-true MPPT techniques like hill-climbing perturbations and observational IC.Finding the MPP with P&O is the easiest and most reliable technique. However, it has three main faults that greatly reduce its usefulness. The method preserves an MPP that was initially fluctuating. Because of the algorithm's architecture, a perturbation is applied that causes the operational point to oscillate with respect to the MPP. Dissipated power is inversely proportional to the size of the first disturbance that sets off the oscillation. Second, when the brightness of the light source increases, the P&O often loses its ability to maintain a steady trajectory. The algorithm starts to deviate from the MPP after it discovers it has been misled into moving in the wrong direction during tracking. It would be a terrible waste of resources if it happened. Third, because of its current design, the P&O is unable to track the partially shaded global peak.

Many scientists have worked hard to find a way to unchain P&O from these constraints. By doing the P&O repeatedly, the steady-state oscillation can be reduced. The divergence problem for rapidly expanding irradiance has not been solved, despite the widespread use of these methods. The issue of divergence and oscillation has been the subject of several recent works, the most prominent of which are [14–16]. The algorithms don't always yield the desired results, and the responses can differ depending on the context. Furthermore, the PV system is subjected to harsh climatic conditions that are not replicated in lab or classroom situations. By creating a very effective adaptive P&O, the problems of steady-state oscillation and divergence have been solved. The oscillation can be found and its effect on the steady-state loss mitigated by keeping an eye on five different perturbation directions. In addition, the tracking is guided in the face of increasing irradiance by use of an adaptive voltage boundary approach. Again, none of these solutions addresses the issue of uneven shading. However, P&O has been the subject of numerous books, essays, and other forms of written media.

May appreciate some cool shade on a hot day. However, neither of these publications deals with oscillation nor divergence at the steady state. This means that none of the solutions presented in the aforementioned books address all three issues simultaneously.When the peak is partially concealed by trees, recent studies have sought to improve global peak location using the P&O by combining it with metaheuristic algorithms including FF, ACO, PSO, and GW. What we have here is a "hybrid" approach. As a result, the P&O has lost some of its classic appeal. Metaheuristic algorithms are a major contributor to the growing computational burden.

A literature search revealed that there is No one P&O method that adequately takes into consideration all three constraints. This research intends to develop an improved adaptive P&O (EA-P&O) by utilizing a dynamic boundary condition, as described in, to dampen steady-state oscillation and get rid of the divergence issue. The algorithm also has the capability of recognizing partial shading situations and quickly searching for the global peak. There is no need for additional temperature or irradiance sensors to obtain real-time updates on open circuit voltage and irradiance data. This makes MPPT much easier to deploy and less expensive than in the past.

II. PV MODELING

There are several different types of PVs that have been documented, the most prevalent of which being single-diode, RS, RP, and two-diode models. In addition to its primary function of circuit simulation, it is compatible with other software programs dealing with electricity, such as MATLAB/Simulink. The two-diode model shown in Fig. 1 allows for more accuracy.

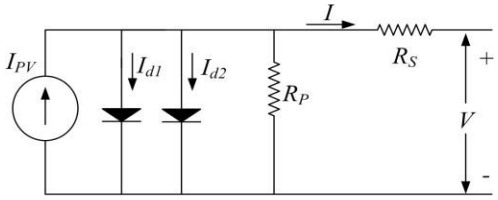

Fig. 1. The two-diode model of solar cells

Two different diode models can be used depending on the system voltage, V, to depict the current being pulled from the PV system.

$$I = I_{pv}N_p - I_{d1} - I_{d2} - \frac{V + IR_s}{NR_p}$$

Where Rs is the series resistance and Rp is the parallel resistance and VT is the diode's thermal voltage.

$$I_{PV} = \left(I_{PV-STC} + K_t(T - T_{src})\right)\frac{G}{G_{src}}$$

Following is the formula for determining the IPV of a light source. It is important to remember that IPV_STC is calculated at STC, or 298 K (250 C), and G=1000 W/m2.Manufacturers frequently include the "KI" short circuit current coefficient. Filling up the Diode current is given by [27]

$$I_{d1} = I_{d2} = \frac{I_{SC\_STC} + K_1(T - T_{STC})}{\exp\left(\left(V_{OC\_STC} + K_V(T - T_{STC})\right)/V_T\right) - 1}$$

In formula (3), Voc and Isc are the STC's open- and short-circuit voltage and current, respectively. The voltage KV coefficient varies with temperature. The PV module used in this work is broken out in detail in TABLE I.

TABLE I: The specifications of the PV module MSX60

Parameters	Label	Value
Short-Circuits currents	I_{SC}	3.8 Amp
Open-circuits voltages	V_{OC}	21.1 Volt
Currents at Pmaximam	I_{MPP}	3.5 Amp
Voltages at Pmaximam	V_{MPP}	17.1 Volt
Max power	P_{MPP}	59.85 Watt
V_{OC} coefficient of temp.	K_V	-0.08 V /ºC
I_{SC} coefficient of temperature	K_I	$3e^{-3}$ A / ºC
Number cell in series per module	n	36

III. THE ENHANCED ADAPTIVE P&O

A. Initialization

The Enhanced Adaptive-P&O reduces steady-state oscillation and locus deviation to allow for continued global peak tracking under obstructive conditions. This is achieved by implementing the full flowchart depicted in Fig. 2. The numerous setup parameters required to start EA-P&O are listed in Table II. For numerical illustration, we use data from the MSX60 PV module.

TABLE II: Initialization Parameters

Parameters	Symbol	Value
OC voltage of a module	V_{OC}	21.1 V
Amount in series	N_S	10
OC Voltage of PV array	V_{oc_array}	211 V
initially perturbation	ΔV	4.22
Initial Voltages of EA-P&O	V_{out}	137.2 V
Steady state flags	steady	0
Oscillation counter	osc	0
Perturbation directions	ϕ	+1
Perturbation counters	slope	[0,0,0,0,0]
Lower Voltage	V_{refl}	10.6 V
Upper Voltage	V_{refh}	200.6 V

B. Tracking under uniform irradiance

The mean posterior proportion (MPP) has been estimated to be close to 0.8Voc_array (where Voc_array=Voc Ns) in numerous investigations. To ensure that MPPT only retains track of a minimal number of perturbation directions before eventually converging on MPP, an initialization of 0.65Voc_array_STC is suggested. The disruption became active at 0.02Voc_array.

Once EA-P&O has been set up, power can be determined by monitoring the PV system's voltage and current. We compare the normalized power (P/P) and (V) with thresholds of 0.1 and 0.005Voc_array, respectively, to ensure that the big power deviation box in Fig. 2 has not been accidentally checked. Due to the fact that P/P can be greater than 0.1 whereas V cannot, the initial outcome of such testing is "no. Scan start when it's greater than 0.005Voc_array. To that end, EA-

P&O has decided to switch to the zero flag. After that point, a small sample size will be all that's needed for MPPT to reach MPP. Once it reaches its maximum power point (MPP), it starts to fluctuate and eventually loses power steadily. EA-P&O can pick up on this kind of oscillation since it follows five different directions of disturbance at once. Then, oscillations are detected using the conditional checking technique described in (4).

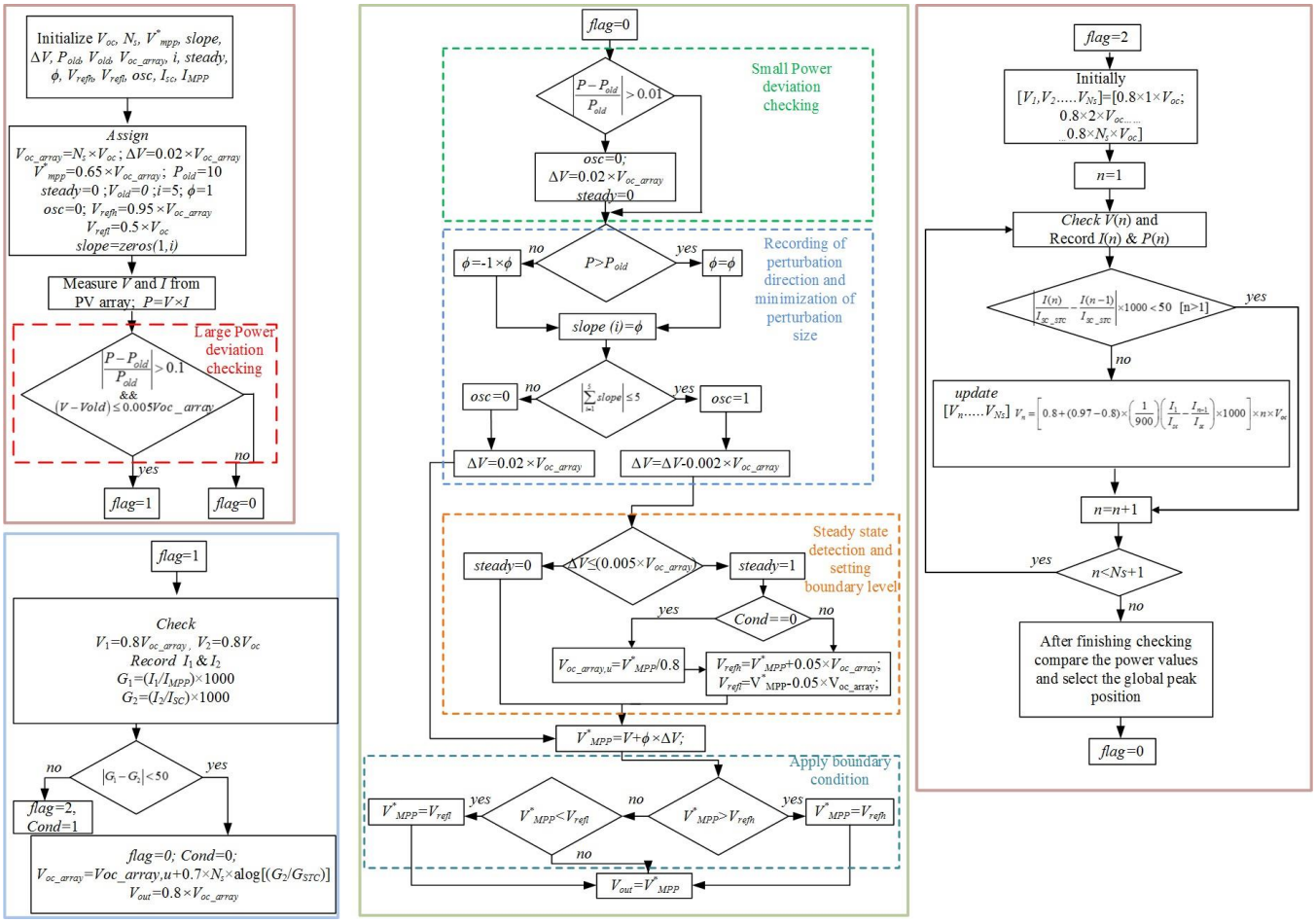

Fig. 2. Comprehensive flowchart for EA-P&O

if $\sum$ slope = $\begin{cases}5 \dots \dots \dots \dots & \text{[MPPT not converged to steady state]}\\ < 5 \dots \dots \dots & \text{[MPPT converged to steady state]}\end{cases}$

When oscillation is found, the size of the disturbance is kept to a minimum by setting it to 0.005Voc_array. So, both the oscillation and the energy waste are cut down. The value of "steady" is changed to 1 as soon as the amount of "disturbance" is brought down to the minimum level. If there is uniform light, the PV grid should have a voltage of MPP (V*) and oscillate with the least amount of change. Many studies have found that in monocrystalline and polycrystalline silicon-based PV modules, MPP happens around 0.8Voc_array.
Such a relationship can also be used to dynamically change the Voc_array as

So, every time EA-P&O follows the MPP, it keeps Voc_array up to date. So, the change in Voc_array caused by temperatures will not affect how well MPPT works.

Also, Voc_array does not need temperature monitors to be constantly updated.

$$V_{\alpha\_\text{array,u}} = \frac{V^*_{M,p}}{0.8}$$

After finding the MPP, EA-P&O put a dynamic boundary condition (DBC) on the operating voltage near the MPP. This made it harder for the operating point to move away from the MPP. As shown in (6), the top boundary is set to Vrefh and the lower boundary is set to Vrefl by 5% of the Voc_array.

$$V_{refh} = V^{*}MPP + 0.05 \times V_{oc\_array}$$
$$V_{refi} = V^{*}\mathrm{MPP} - 0.05 \times V_{\mathrm{oc\_array}}$$

Conventional P&O tends to go in an opposing direction from the MPP when G starts to rise gradually and quickly. When this happened, the efficiency went down by 10% to 50%, based on how G ramped up [16]. As shown in Fig. 3, a border condition keeps the operating point from moving away from the MPP trail.

After settling on MPP with a limited voltage boundary, there are four different situations that could happen:
a) The amount of light will slowly change (increase or drop).
b) The temperature will change.
c) a quick, big change in the amount of light.
d) the appearance of partial shading.

During case (a), if the rate of change of light (G/t) is less than 10 W/m2/s, the divergence problem doesn't hurt the performance of the MPPT. But if (G/t) is more than 10 W/m2/s, standard P&O moves away from the MPP locus, which leads to a big loss of power. When G begins to vary, the mathematical relationship between two successive MPPT-scanned samples is as shown in [19

$$\frac{\Delta P}{P} = \frac{\Delta G}{G_{STC}}$$

So, if $\Delta G/\Delta t$ is less than or equal to 10 W/m2/s, the threshold for normalized power can be calculated as $\Delta P/P = \Delta G/G_{STC}$ = (10/1000) = 0.01. If ΔP/P is more than 0.01 as shown in Fig. 2, EA-P&O will keep checking within flag 0. If it's much larger than this, EAP&O will consider the possibility of a rapid shift in the solar output. To ensure that the voltage can travel through the MPP route, we reset the disturbance size to its initial value of 0.02Voc_array and set the'steady' variable to 0. Caused by a significant shake. The MPP trail is losing its grip on power. Figure 3 shows, however, that the upper and lower boundary conditions maintain a constant voltage level very near to the MPP. Therefore, the issue of power loss as a result of separation has been resolved.

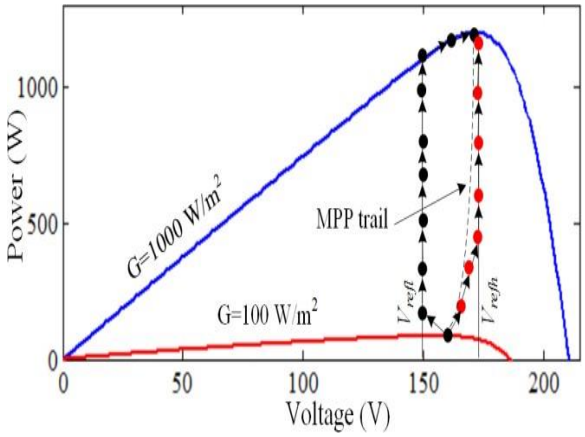

Fig. 3. Restricting operating voltage near MPP

When the temperature changes (condition b), this involves a very slow process which spans several hours. But the temperature changes Voc_array in a big way. Since EA-P&O modifies Voc_array with (5), a variation in temperature doesn't affect how well MPPT works.

If (c) or (d) take place, an instantaneous alteration in irradiance or partial shading is usually found by a big change in the power variation. Most MPPT algorithms can't tell the disparity between these two scenarios, as shown in [30, 31]. When they see a big change in power, they begin searching for globally peaks under the partial shading, even though partial shading isn't taking place at that particular moment.

These brief variations in power can be found by EA-P&O's "big power deviation" block. When the criterion is fulfilled, the EA-P&O sets off Flag 1. Then, EA-P&O checks at two particular voltages on the curve: V1=0.8Voc_array and V2=0.8Voc. In the present situation, V1 is close to the MPP and V2 is at the current flowing through the short circuit point. So, I1, which stands for IMPP, and I2, which stands for ISC, are the two points where the current is recorded. Following that, you may employ both of these present values for figuring out the irradiance different levels (G) on the I-V curve outlined in [30].

When $I_1=I_{MPP}$

$$G_1 = \frac{I_{MPP}}{I_{MPP\_STC}} \times G_{STC}$$

At $I_2 = I_{SC}$

$$G_2 = \frac{I_{sc}}{I_{SC\_STC}} \times G_{STC}$$

This plan can be checked with numbers by employing the example that follows. Figure 4 shows the I–V graph for three levels of light (1000 Watt/m^2, 600 Watt/m^2, and 300 Watt/m^2). The current associated with I_{SC}=I0.8Voc while the IMPP=I0.8Voc_array are indicated on the curve. At STC, the I_{SC} rating for the MSX 60 PV module is 3.8 A as well as the IMPP is 3.5 Amps. At 1000 Watt/m^2, you can use equations (8) and (9) to figure out G1 and G2.
At I_{MPP} and I_{sc}

$$G_1 = \frac{I_{MPP}}{I_{MPP\_STC}} \times G_{STC} = \frac{3.542}{3.5} \times 1000 = 1012$$
$$G_2 = \frac{I_{SC}}{I_{SC\_STC}} \times G_{STC} = \frac{3.782}{3.8} \times 1000 = 995.3$$

G1 and G2 are both extremely near to the target value of 1000 W/m2 as can be observed. Nevertheless, there is a 17-point discrepancy in the values.

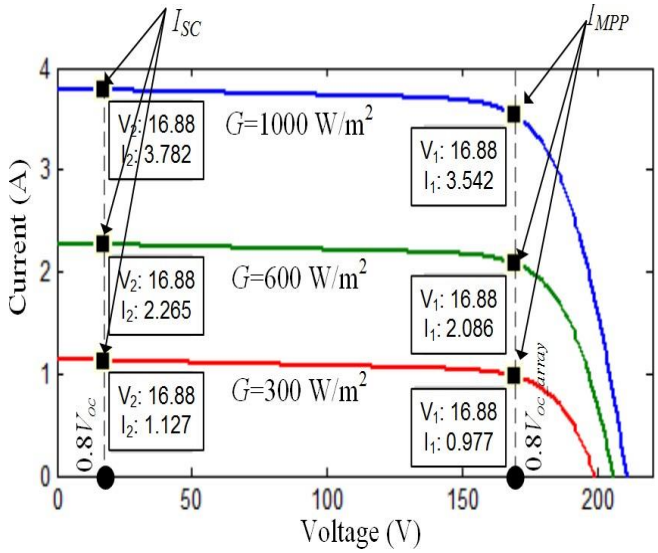

Fig. 4: Characteristics of *I–V* curve during uniform irradiance

Similarly, when referencing the I-V curve for 600 W/m2, the numbers for G1 and G2 add up to 596 W/m2, with no discrepancy. At 300 Watt/m^2, the computed value for G1 is 296 W/m2, whereas the value for G2 is 279 W/m2, a difference of 17. An significant conclusion can be drawn from these findings: after G1 and G2 are determined and the disparity remains below a threshold, the algorithm considers the condition to have uniform irradiance. According to [30], Monocrystalline and polycrystalline solar panels usually have a G1-G2 absolute disparity of a value below 40 under standard illumination conditions. Thus, in Fig.2, the disparity between G1 and G2 is determined by verifying the first flag. However, the cutoff has been raised to 50 from 40 so that there would be some room for error. If the variation in uniform irradiance is what's causing the power to fluctuate widely, then |G1-G2| will stay below 50 and we won't be talking about partial shading.When the amount of irradiance fluctuation is large & consistent, partial shading checking is unnecessary. Rather, EAP&O begin with 0.8Voc_array, which is expected for MPP, after adjusting Voc_array and Voc by (10), as illustrated in [30].

$$V_{\text{oc\_array}} = V_{oc\_\text{array, ,u}} + aV_tN_s\ln\left(\frac{G_1}{G_{STC}}\right)$$
$$V_{\text{oc}} = V_{\text{oc\_array}}/N_s$$

Then, it begins P&O with flag 0 and accurately follows the MPP while limiting the amount of any perturbations. Setting

the 'cond' variable to 0 indicates uniform irradiance situation. The opposite is true whenever partial shading is present.

Then the value "1" is put in the "cond" variable, and EA-P&O starts flag 2 (in Figure. 2), in which it attempts to locate a global peaks while partially shading

C. *Scanning Under partial shading*

There are several locations whereby the surrounding summits appear when there is some partial shading. The 0.8Voc model [20, 21] says that local peaks should be close to the multiples of 0.8Voc. So, it is easy to find the world peak by comparing the power of the voltages that are at multiples of 0.8Voc. But [32] shows that as the shade level went up Increasing the total amount of modules in sequence shifts the local peak voltages towards the right, creating a large delta from 0.8Voc multiples. So, to make it more accurate, it's important to move the projected points to the right and make the shading level higher. So, a better scanning method is created and added to EA-P&O. The graph shown in Fig. 5 is used to explain how the process works. There are 10 units in a row, and each one gets a dose of 1000, 600, 400, or 200 W/m2. Under each level of brightness, there are 3, 2, 2, and 2 units, respectively. The positions of the objects inspected by the 0.8Voc models can be seen in Figure 5(a). Scanning each point derived from the 0.8Voc model reveals that location I4 corresponds to the LP1. The problem is that the I6 and the LP2 are not aligned. While I9 was able to locate LP3, LP4 has yet to be scanned. The reason for this is due to the peaks are shifting to the right.

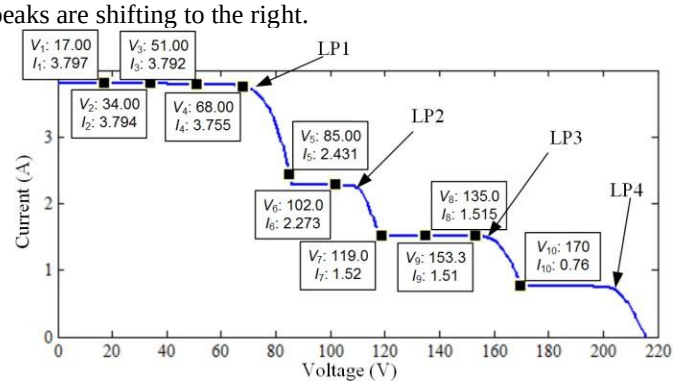

(a)

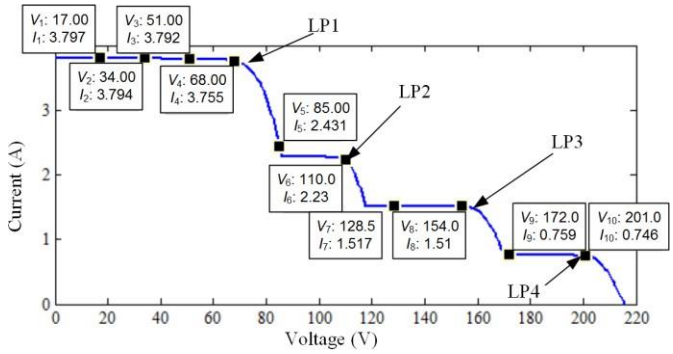

(b)

Fig. 5: (a) predicted points by 0.8Voc model (b) predicted points by EA-P&O.

Scanning of the EA-P&O is shown in Fig. 5(b). EAP&O starts by screening the 0.8Voc points by giving them the values [V1,V2.....VNs]=[0.81Voc, 0.82Voc.....0.8NsVoc]. The short circuit current is close to the first point that was scanned (V1, I1). Using equation (9), the G at the first step of the current is calculated to be 1000 W/m2. The data from point I2 is then saved in variable V2. Calculating G at I2 employing (9) and comparing it to G at I1 reveals that they are extremely similar (the difference is less than 50). In this respect, I3 and I4 are interchangeable. EA-P&O initial believed that the current level was on the first stair until it scanned (V5, I5) and calculated G as (2.43 / 3.8)=639.5 W/m2. As a result, the remaining estimated peak positions must be shifted to the right. Through a conceptual shift in [32], the following equation can be used to figure out the local peak point when right shifting is taken into account.

$$V_n = \left[0.8 + (0.97 - 0.8) \times \frac{1}{900} \times \left(\frac{I_1}{I_{sc\_STC}} - \frac{I_{n-1}}{I_{SC\_STC}}\right) \times 1000\right] \times n \times V_{oc}$$

According to the (11) new predicted positions are

$$V_6 = \left[0.8 + (0.97 - 0.8) \times \frac{1}{900} \times \left(\frac{I_1}{I_{SC\_STC}} - \frac{I_{n-1}}{I_{SC\_STC}}\right) \times 1000\right] \times 6 \times V_{oc}$$

$$V_6 = \left[0.8 + (0.97 - 0.8) \times \frac{1}{900} \times \left(\frac{3.797}{3.8} - \frac{2.43}{3.8}\right) \times 1000\right] \times 6 \times 21.1 = 109.88$$

As a result, the V6 is shifted to 110 V, and this puts it squarely on the LP2. V7 has reached 128.5 V (up from 119 V in the 0.8Voc version) as a result of the shift to the right. When the irradiance levels fluctuate, EA-P&O shifts the remaining peaks. In any case, (11)

$$V_8 = \left[0.8 + (0.97 - 0.8) \times \frac{1}{900} \times \left(\frac{I_1}{I_{SC\_STC}} - \frac{I_{8-1}}{I_{SC\_STC}}\right) \times 1000\right] \times 8 \times V_{oc}$$

$$V_8 = \left[0.8 + (0.97 - 0.8) \times \frac{1}{900} \times \left(\frac{3.797}{3.8} - \frac{1.517}{3.8}\right) \times 1000\right] \times 8 \times 21.1 = 154.1$$

Therefore, V8's release of the LP3 is spot-on. The exact same scenario will occur if V9 is measured at 172 V and V10 is changed to 200 V. That is where LP4 really is, as shown in Fig. 5(b). One can come to the conclusion that if the right shifting mechanism is used, predictions about where local peaks will be are more correct. The scanned power will be compared after all the properly predicted peaks have been scanned. Based on the values, the world peak will be the place that gives off the most power.

IV. RESULTS AND DISCUSSIONS

Hardware as well as the Simulink environment for EA-P&O are configured as indicated in [19]. The two-diode model is used to set up the program. The model is given the values of T and G, and The converter that receives the photovoltaic current. In order to adapt the voltage that comes obtained the the MPPT outputs to the loads voltage, a buck-boost dc-to-dc converter is used. Considering the values of f = 50 kHz, L = 1 mH, and C1 = 470 F and C2 = 220 F, the converter is designed to operate within the continual inductor current state.

A. Simulation results

Rapid irradiance changes, fast-gradient irradiance changes with an average gradient about 20 W/m2/s, and partial shade are all a component of the battery of tests used to evaluate the EA-P&O. A set of ten modules (MSX 60) is put through a test that make up a PV array. In parallel, two strings that are the same are linked. Figure 6 shows how G changes for a 10 s.

Following that, beginning at 65 s, G increases at a slope of 20 W/m2/s till the value reaches 1000 W/m2. After which, for another 10 seconds, it will maintain a constant 1000 W/m2. As soon as the 75 seconds mark has passed, partial coloring will begin.

Figure 6(b) depicts the partial shading graph. There are four types of shading applied to the PV array: (1000, 800, 600, and 400W/m2), which is shown by the curve's four points. 15 s are spent with the limited shading.

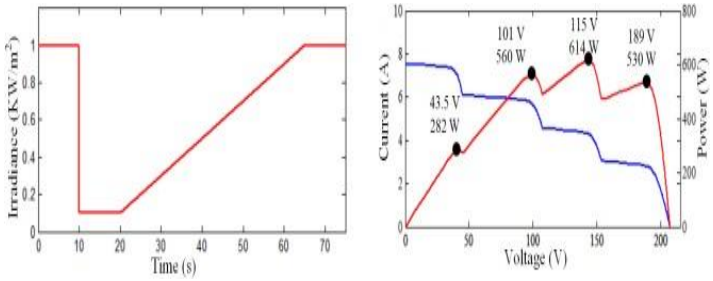

(a) (b)

Fig. 6: (a) Variation of irradiance vs. time (b) *P–V* (red)

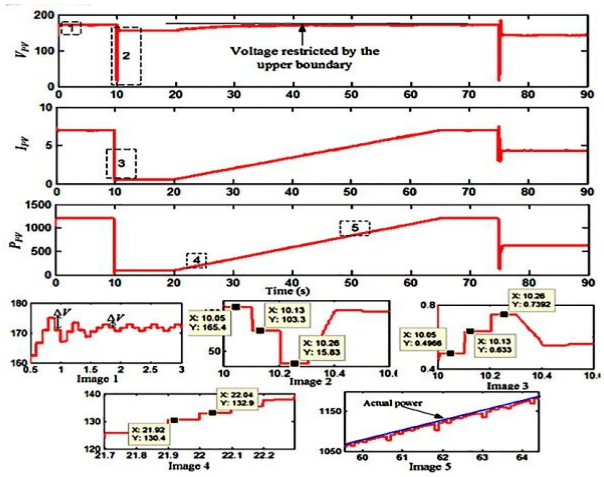

Therefore, the most recent prediction for G's Voc_array value (100
W/m2) is 194.69V. The EA-P&O immediately resumes its original course of operation at 155.75 V (194.69 – 0.8 = 155.75) in compliance with the MPP. Standard Maximum Power Point Tracking techniques will only give it partial credit if no such ingenious way exists.

$$V_{\text{oc\_array}} = 211 + 1 \times 0.7 \times 10\ln\left(\frac{97.4}{1000}\right) = 194.69$$
$$V_{oc} = 194.69/10 = 19.47$$

Voc_array for a given G (100 W/m2) has thus been recalculated to with a value of 194.69V. Later then, the EA-P&O resumes its previous MPP tracking at 156 V (194,690.8=155.75 V). If there wasn't such a smart mechanism, the normal MPPT scheme would treat it as a case of partial shading and start an unnecessary global peak search.

After 20s, G starts going up with a 20 W/m2/s slope. Figure 7's PPV curve shows that the EA-P&O closely follows the MPP path instead of going in different directions like traditional P&O. Two parts of the PPV are blown up in Images 4 and 5 so that you can understand them better. According to equation (7), when G is 20 W/m2, P/P should be 0.02. Image 4 shows that this is true. In two measures of power that come one after the other, P1 and P2 are each 130.4 and 132.9. So, it is worked out as

$$\frac{\Delta P}{P} = \frac{P_2 - P_1}{P_1} = \frac{132.9 - 130.4}{130.4} = 0.019 \approx 0.02$$

Figure 7: The VPV, IPV, and PPV profiles of the EA-P&O's movement. Some of the curves have been magnified so that you can more clearly see how the algorithm reacts during transitions. The first picture shows that the initial perturbation in EA-P&O is quite large (0.02Voc_array). When the MPP is hit, immediate action will be taken (15.87) V. Where x is time, images 2 and 3 depict the scan's voltage and current, respectively. Both the low voltage range (103.3 V) and the high voltage range (165.7 V to 15.87 V) are checked. The PI controller requires additional voltage scanning to allow operation from 165.7 V down to 15.87 V. Information gathered at 103.3 V, however, is never saved or used in any way.The current values are shown in Figure 7.

Both 0.8Voc_array and 0.8Voc generate currents of 0.74 A. EA-P&O followed the instructions and powered on the MSX 60 modules at ISC = 3.8 A and IMPP = 3.5 A. Isc is 7.6 A and IMPP is 7 A since two module strings are used in this study. Power levels of G1 (0.5/7100=71.4 W/m2) and G2 (0.74/71000=97.36 W/m2) can be measured by scanning at EA-P&O. These two G values differ by about 25 W/m2. Given that the discrepancy is less than 50, EA-P&O will consider it to be the result of a shift in G rather than any detectable variation in shading. The Voc_arry and Voc will be recalculated by a factor of 10 after EA-P&O is informed of the new irradiance level. EA-P&O can detect the magnitude of the disturbance (V) and initiate damping processes. As a result, EA-P&O will be relocating to the

Fig. 7: Tracking profile of EA-P&OEA-P&O's G drops to 100 W/m2 after following the MPP for just 10 seconds. Large normalized power increases due to G are a clear indication that (P/P) is more than 0.1. Since the need for tracking significant power fluctuations has been satisfied, partial shading occurrence verification can proceed (flag 1). By taking the aforementioned measures, the EA-P&O can examine points on the curve at coordinates 0.8Voc_array (165.7) V and 0.8Voc_array (165.7) V.

The voltage ceiling is larger than 0.01 but less than 0.1, limiting the usable operating range. The VPV indicates that the voltage is too high after only a few seconds. After that point, the voltage must remain relatively constant close to the MPP in accordance with the boundary limit. Therefore, we no longer have to worry about the divergence issue. The measured voltage is not anticipated to be precisely on the MPP, but it should remain close to it. Photo 5 shows that the reported output is less than the real one. Although efficiency has dropped by a fraction of a percentage point, it is still quite near to 99.5%.

After seventy-five seconds, there's a brief dimming, followed by a slow shift in G. From 75 s to 77 s, Figure 8 depicts EA-P&O's transient tracking while partially obscured. In can Check the partial shade as shown in the VPV by EA- P&O by scanning the 0.8Voc_array (165.91 V) and 0.8Voc (15.88 V). Currents at 0.8Voc_array (2.98 A) and 0.8Voc (7.477 A) can be calculated with IPV. The EA-P&O determined that the G1 and G2 were 425 W/m2 and 983 W/m2, respectively, at 0.8Voc_array and 0.8Voc. There is a difference of around 50 in G, or 558 W/m2. This has led to EA-P&O's decision to look into the prospect of partial shading.

EA-P&O employs a search strategy predicated on the 0.8Voc model. V-values of 16.88, 33.76, 50.64, 67.52, 84.42, 101.28, 118.16, 135.04, 151.92, and 168.81 are targeted by EA-P&O for this particular template. According to the VPV curve depicted in Fig. 8, EA-P&O accurately scans the first three spots, however the fourth point is incorrectly placed at 70.27 V, when it should be at 67.52 V. An upward trajectory toward the summits.

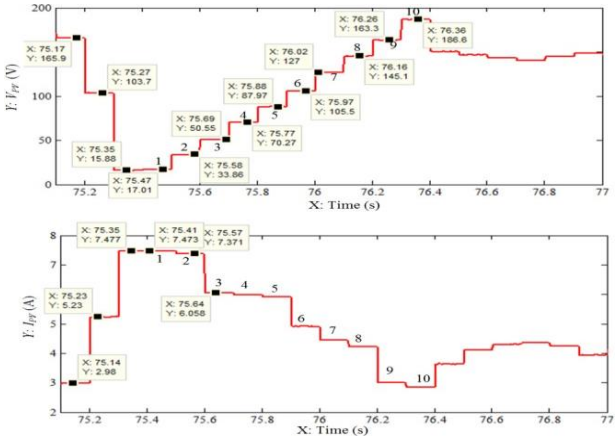

Fig. 8: EA-P&O tracking under partial shading

Taking into account the modern notations on the IPV curve is crucial to grasping the full scope of the procedure. Samples 1 and 2 currently have values that are very close to each other, whereas sample 3 has a level that is significantly lower. EA-P&O find a decrease in current between levels 1 and 2 after scanning a third sample. According to the formula in (11) V = 0.8 0.97 0.8 1 I1 In1 1000V n, EA-P&O move the position of the remaining peaks to the right.

$$V_n = \left[0.8 + (0.97 - 0.8) \times \left(\frac{1}{900}\right) \times \left(\frac{I_1}{I_{sc}} - \frac{I_{n-1}}{I_{sc}}\right) \times 1000\right] \times V_{oc} \times n$$

$$V_4 = \left[0.8 + (0.97 - 0.8) \times \left(\frac{1}{900}\right) \times \left(\frac{7.371 - 6.058}{7.6}\right) \times 1000\right] \times 21.1 \times 4$$

$$V_4 = 70.28$$

The current levels in samples 3, 4, and 5 are pretty close, but in sample 6 they drop by a lot. Because of this, the changes in gear ratios for the V7, V8, V9, and 10 engines are all the same. The IPV graph in Sample 9 shows another sharp drop. After EA-P&O checked the drop in power, the V10 was moved to the fourth floor.

This shift to the right side puts the scanning maximum nearer to the actual localized peaks, as shown in Figure 6(b) of the PS curve. While looking to identify the genuine worldwide top beneath partial shading, EA-P&O uses this innovative right sliding mechanism to verify the greatest power extracting possible.

B. Comparing the different MPPT methods

Four state-of-the-art MPPT approaches, including the customized incremental conductance procedure (MIC) [33], the artificially created bee colony (ABC) [5], the cuckoo searching (CS) [8], including a hybrid strategy combining P&O with the ant colony optimizing (ACO-P&O) [4], are compared to the efficiency of the suggested EA-P&O. We selected the metaheuristic ABC, the heuristic CS, and the ACO-P&O to test the efficacy of EA-P&O, along with the heuristic MIC, a flexible take on the traditional MPPT., which is a mixed MPPT scheme. A 105-S-P pattern made out of MSX60 modules generates the I-V and P-V curves. Figure 9 shows the results of applying these steps to three partial shading curves with different MPP positions. There are three peaks along the -axis of voltage, with the global maximum (GMPP1) located in the middle. A first-degree partial shading design. The four-peak GMPP2 for the PS2 can be found farther to the left. Towards the right end of the partial shading (PS3) graph is where you'll find the GMPP3. There are five summits altogether. The first second of each test series employs uniform irradiance, whereas the next three employ partial shading curves with durations of two seconds each.

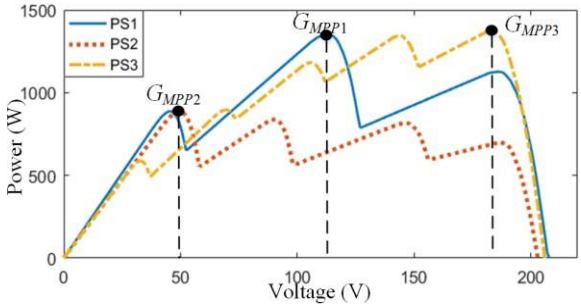

Fig. 9: Partial shading curves for performance evaluation of EA-P&O against four different MPP techniques

250 ms. For GMPP1, ten samples are required for detection. The MIC co-localizes with GMPP1 in this region.

The remaining variables' values will also be adjusted such that the final sum is 87.96. EA-P&O is narrowing in on the projected sweet spot for V4, V5, and V6 based on the VPV curve (105.55, 123.14, 140.74, 158.33, 175.92). However, the V7 has received yet another upgrade, and the voltage will now be 127 V instead of 123.14 V. The IPV curve demonstrates this theory. This is only one instance of somewhat comparable time intervals. Comparatively, the ACO-P&O only needs 22 samples (550 ms) to converge on the GMPP1, while the ABC needs 30 samples (750 ms). Because of how randomly ABC and ACO-P&O seek, transient variations tend to be larger. CS is significantly faster than both ABC and ACO-P&O. This concludes the discussion.

Using the Levy flight, CS is able to achieve convergence more quickly than other metaheuristic algorithms. In comparison to EA-P&O and MIC, its slowness was to be expected. All algorithms, save for CS, correctly report the current worldwide PS2 peak. It has already been shown that CS search agents can employ Levy flights to quickly reach the area's prime spots. If the CS agents place GMPP2 too far to the left, they risk missing the global peak. Both EA-P&O and MIC are comparable to GMPP2 after 10 samples. Both ABC and ACO-P&O are time-consuming procedures due to the large number of samples they require (32 and 24, respectively). Please keep in mind that MIC does not keep track of the global maximum of PS3 (GMPP3). Due to the limitations of the 0.8Voc model upon which the MIC is based, it can only scan up to a maximum of 1Voc. For the 0.8Voc model (100.8Voc=168.8 V), GMPP3's voltage is too high. So, we can't go over the transient peak voltage of 140 V. The EA-P&O gets around this problem by employing the optimal shifting technique as out in III©. A peak voltage of 140 V in the area is sufficient to ensnare both CS and MIC. In terms of GMPP3 monitoring, EA-P&O is faster than ABC and ACO-P&O, but all three methods are still reliable.

Figure 7 depicts the EA-P&O's VPV, IPV, and PPV velocity, acceleration, and direction profiles. Some of the curves have been magnified to better show how the algorithm works with data. There is a major disruption in EA-P&O (0.02Voc_array) in the first picture. If the MPP is broken, urgent action will be taken (15.87) V. The voltag**e is** shown in Image 2, and the current in Image 3. There is an examination of both high and low voltage (beginning at 103.3 V and going all the way down to 15.87 V). Further voltage scanning of the PI controller is required for operation from 165.7 V down to 15.87 V. Information is gathered at 103.3 V, however it is never used or stored.

The current values are depicted in Figure 7.Currents of 0.74 A are generated by both 0.8Voc_array and 0.8Voc. The MSX 60 modules were activated through EA-P&O with ISC = 3.8 A and IMPP = 3.5 A. Both the Isc 7.6 A and the IMPP 7 A are the result of two module strings. Radiation levels in both G1 (0.5/7100=71.4 W/m2) and G2 (0.74/71000=97.36 W/m2) can be calculated using scanning at EA-P&O. These two G values differ by about 25 W/m2. Given that the discrepancy is under 50, EA-P&O will treat it as a change in G rather than a noticeable shift in tone. After EA-P&O receives the new irradiance reading, they will increase Voc and Voc_arry by a factor of 10
EA-P&O can be utilized to commence damping operations once the magnitude of the disturbance (V) has been established. Therefore, the firm has resolved to relocate to

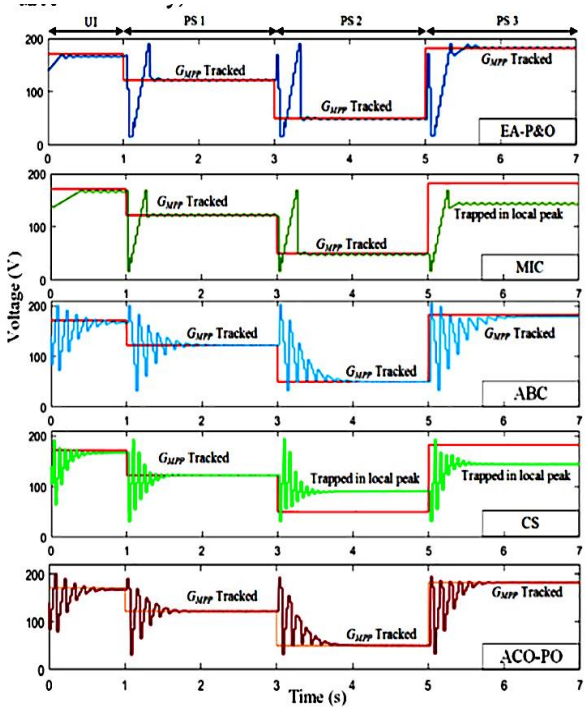

Fig. 10: Voltage profile for EA-P&O, MIC, ABC, CS & ACO-P&O

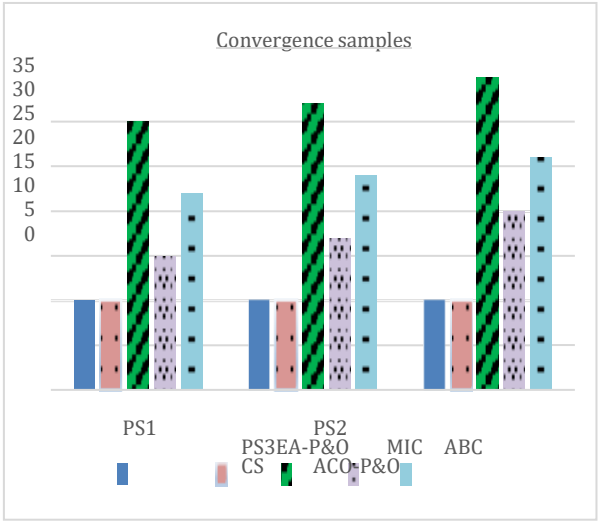

Fig. 11: **Convergence samples of all five MPPT algorithms under partialshading**

The required sample size to reach convergence is depicted in Figure 11. When compared to MIC, the proposed method is night and day.Better efficiency than competing algorithms. While the inability to detect GMPP3 suggests that the MIC is just as fast, it is not certain that the GMPP can be followed under any given partial shade curve.

Table III provides a summary of further differences between the two methods. In metaheuristic approaches, such as ABC and ACO-P&O, the number of search agents is always balanced against the likelihood of convergence. ABC and ACO-P&O often use a large number of agents (five or six) to get convergence in partial shade. Tracking will slow down when more agents are used, but more global peaks will be detected. CS's three-agent setup reduces administrative burden and increases throughput. The fact that GMPP2 is not detected raises doubts about its accuracy.

When compared to ACO-P&O, which only requires a single tuning parameter, ABC and CS require two in order to achieve their full performance potential. The parameters of EA-P&O and MIC can be set once, making their implementation in code simpler. Since EA-P&O is a voltage-based MPPT algorithm, it can only work with STC data provided by the manufacturer. The parameters VOC, ISC, and IMPP (at STC) all decline with module age. Therefore, the STC values need to be reevaluated on a regular basis. Even more so in computer science. However, EA-P&O and CS, being voltage-based algorithms, are unaffected by load change. As a result, there will be less short-term fluctuations in tracking. The MIC, the ABS, and the ACO-P&O all rely on direct duty cycle MPPT to function. This shields them from the natural decline in sensibility that occurs with age. However, as pointed out by [33], duty cycle based algorithms have the unfortunate tendency to be badly impacted by periodic load variations.

Table III: Table comparing EA-P&O with different MPPT methods

Parameters	EA-P&O	MIC	ABC	ACO-P&O	CS
GMPP tracking guaranteed	Y	N	Y	Y	N
Convergence samples (millisecond)	10	10	30-35	22-26	15-20
Convergence time (millisecond)	250	250	625-750	750-875	375-500
Complexity	Medium	Medium	High	Medium	High
Tuning parameter	None	None	2	1	2
Reliability	High	Medium	High	High	Medium
System dependency	Y	N	N	N	Y
Load dependency	N	Y	Y	Y	N

The EA-P&O has kept to its simple, classic design. It's easier to implement than metaheuristic strategies. Sensors for light and temperature are also superfluous.

A. Evaluation of Hardware for Partial Shade By constructing a buck-boost converter and a Dspace platform (using the DS1104 board), we can test EA-P&O's efficacy. A simplified diagram of the hardware configuration is provided in Fig. 12. Three partial shadow curves are utilized to evaluate the efficiency of the PV array in Fig. 13. The series prototype's four modules served as inspiration for the final hardware design. The P-V curve can have no more than four distinct peaks. You can see how wonderfully it functions right now.

Starts off with a constant glow on the screen. The first waveform has a single peak at 68V, indicating a constant brightness. After that, curve 2's partial shading pattern will take its place, making the lighting less even overall. A maximum of 72 V was measured. The transition from partial shade to uniform irradiance can be better understood if uniform irradiance is introduced again. The third curve then takes on some of its former brightness. The highest of the other four peaks is a 52-volt offset worldwide peak. Curve 1 can now be seen in its entirety after being partially hidden for long time. When the global peak voltage reaches 34 V, curve 4 begins to partially darken for the last time.

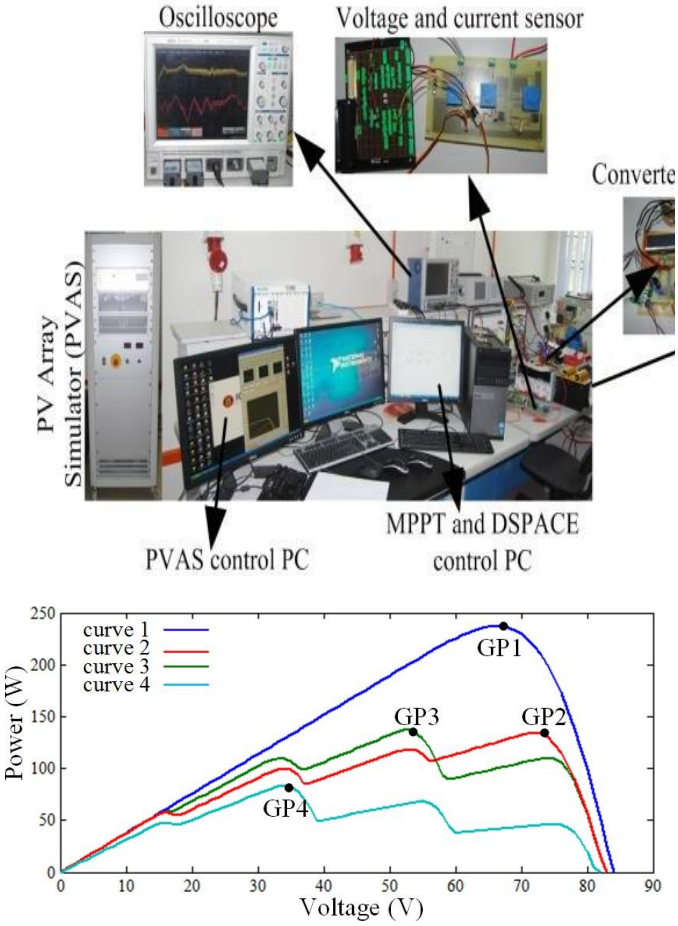

Fig. 13: Partial shading patterns applied in the hardware

The EA-P&O tracking oscillogram is shown in Figure 14. According to the VPV data, EA-P&O initially employs the MPP to suppress the steady-state oscillations. EA-P&O will commence additional monitoring in two locations if it detects partial shadowing along curve 2. After doing all of the relevant tests, EA-P&O verifies the presence of partial shading by scanning the P-V curve. The peak voltage is calculated to be 72 V by averaging the voltages at the curve's four vertices. This makes it possible to effectively adhere to GP2.

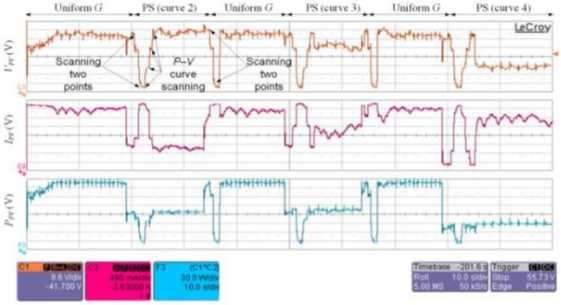

Fig. 14: Tracking profile of EA-P&O from oscilloscope

The sun's rays will return to their regular patterns after this point, and the balance of power will shift dramatically away

from EA-P&O and toward the rest of the planet. That's why it falls back to contrasting the shade levels of two points on the curve, as was the case originally. The EA-P&O relocate to a spot where the PV module receives the same amount of light after recalculating the Voc_array. Curves 3 and 4 could share several behavioral characteristics. The lowest recorded voltage was 33 V, while the highest was 52 V, according to EA-P&O's investigation.

V. CONCLUSION

As a full solution to the issues with traditional P&O, we suggest a new MPPT technique in this study. Energy loss due to partial shading, divergence, and steady-state oscillation could be reduced using the proposed method. Whether or not irradiance and temperature sensors are present, the open circuit voltage is likewise routinely updated. This technique for detecting partial shadowing is quite precise and has the potential to reduce peak scanning and energy costs on a worldwide scale. The algorithm's behavior has been elucidated thanks to exhaustive simulation and hardware discoveries, which explain its operation and guarantee an efficiency of over 99% regardless of environmental conditions. This algorithm may be the best option for overcoming the practical challenges of MPPT. Keep in mind that the initialization phase of a controller requires the setting of various function parameters. The I-V and P-V properties of monocrystalline and polycrystalline PV modules were also considered during the design process. This eliminates the option of using thin film modules to implement EA-P&O.

VI. REFERENCES

[1] H. Renaudineau *et al.*, "A PSO-Based Global MPPT Technique for Distributed PV Power Generation," *Industrial Electronics, IEEE Transactions on,* vol. 62, no. 2, pp. 1047-1058, 2015.

[2] M. Seyedmahmoudian *et al.*, "Simulation and Hardware Implementation of New Maximum Power Point Tracking Technique for Partially Shaded PV System Using Hybrid DEPSO Method," *IEEE Transactions on Sustainable Energy,* vol. 6, no. 3, pp. 850-862, 2015.

[3] K. Punitha, D. Devaraj, and S. Sakthivel, "Artificial neural network based modified incremental conductance algorithm for maximum power point tracking in photovoltaic system under partial shading conditions," *Energy,* vol. 62, pp. 330-340, 2013.

[4] K. Sundareswaran, V. Vigneshkumar, P. Sankar, S. P. Simon, P. S.

a. R. Nayak, and S. Palani, "Development of an improved P&O algorithm assisted through a colony of foraging ants for MPPT in PV system," *IEEE Transactions on Industrial Informatics,* vol. 12, no. 1, pp. 187-200, 2016.

[5] K. Sundareswaran, P. Sankar, P. S. R. Nayak, S. P. Simon, and S. Palani, "Enhanced Energy Output From a PV System Under Partial Shaded Conditions Through Artificial Bee Colony," *IEEE Transactions on Sustainable Energy,* vol. 6, no. 1, pp. 198-209, 2015.

[6] S. Mohanty, B. Subudhi, and P. K. Ray, "A new MPPT design using grey wolf optimization technique for photovoltaic system under partial shading conditions," *IEEE Transactions on Sustainable Energy,* vol. 7, no. 1, pp. 181-188, 2016.

[7] D. Teshome, C. H. Lee, Y. W. Lin, and K. L. Lian, "A Modified Firefly Algorithm for Photovoltaic Maximum Power Point Tracking Control Under Partial Shading," *IEEE Journal of Emerging and Selected Topics in Power Electronics,* vol. PP, no. 99, pp. 1-1, 2016.

[8] J. Ahmed and Z. Salam, "A Maximum Power Point Tracking (MPPT) for PV system using Cuckoo Search with partial shading capability," *Applied Energy,* vol. 119, no. 0, pp. 118-130, 4/15/ 2014.

[9] J. Ahmed and Z. Salam, "A critical evaluation on maximum power point tracking methods for partial shading in PV systems," *Renewable and Sustainable Energy Reviews,* vol. 47, no. 0, pp. 933-953, 7// 2015.

[10] K. Ishaque and Z. Salam, "A review of maximum power point tracking techniques of PV system for uniform insolation and partial shading condition," *Renewable and Sustainable Energy Reviews,* vol. 19, no. 0, pp. 475-488, 3// 2013.

[11] S. K. Kollimalla and M. K. Mishra, "Variable perturbation size adaptive P&O MPPT algorithm for sudden changes in irradiance," *Sustainable Energy, IEEE Transactions on,* vol. 5, no. 3, pp. 718- 728, 2014.

[12] S. K. Kollimalla and M. K. Mishra, "A novel adaptive P&O MPPT algorithm considering sudden changes in the irradiance," *Energy Conversion, IEEE Transactions on,* vol. 29, no. 3, pp. 602-610, 2014.

[13] F. Zhang, K. Thanapalan, A. Procter, S. Carr, and J. Maddy, "Adaptive hybrid maximum power point tracking method for a photovoltaic system," *Energy Conversion, IEEE Transactions on,* vol. 28, no. 2, pp. 353-360, 2013.

[14] F. Paz and M. Ordonez, "Zero oscillation and irradiance slope tracking for photovoltaic MPPT," *Industrial Electronics, IEEE Transactions on,* vol. 61, no. 11, pp. 6138-6147, 2014.

[15] M. Killi and S. Samanta, "Modified Perturb and Observe MPPT Algorithm for Drift Avoidance in Photovoltaic Systems," *Industrial Electronics, IEEE Transactions on,* vol. 62, no. 9, pp. 5549-5559, 2015.

[16] T. Bennett, A. Zilouchian, and R. Messenger, "A proposed maximum power point tracking algorithm based on a new testing standard," *Solar Energy,* vol. 89, pp. 23-41, 2013.

[17] A. Pandey, N. Dasgupta, and A. K. Mukerjee, "High-performance algorithms for drift avoidance and fast tracking in solar MPPT system," *Energy Conversion, IEEE Transactions on,* vol. 23, no. 2, pp. 681-689, 2008.

[18] E. Mamarelis, G. Petrone, and G. Spagnuolo, "A two-steps algorithm improving the P&O steady state MPPT

efficiency," *Applied Energy,* vol. 113, no. 0, pp. 414-421, 1// 2014.
[19] J. Ahmed and Z. Salam, "A Modified P&O Maximum Power Point Tracking Method With Reduced Steady-State Oscillation and Improved Tracking Efficiency," *IEEE Transactions on Sustainable Energy,* vol. 7, no. 4, pp. 1506-1515, 2016.
[20] H. Patel and V. Agarwal, "Maximum Power Point Tracking Scheme for PV Systems Operating Under Partially Shaded Conditions," *Industrial Electronics, IEEE Transactions on,* vol. 55, no. 4, pp. 1689-1698, 2008.
[21] A. Kouchaki, H. Iman-Eini, and B. Asaei, "A new maximum power point tracking strategy for PV arrays under uniform and non-uniform insolation conditions," *Solar Energy,* vol. 91, no. 0, pp. 221-232, 5// 2013.
[22] C. Kai, T. Shulin, C. Yuhua, and B. Libing, "An Improved MPPT Controller for Photovoltaic System Under Partial Shading Condition," *Sustainable Energy, IEEE Transactions on,* vol. 5, no. 3, pp. 978-985, 2014.
[23] C. Manickam, G. P. Raman, G. R. Raman, S. I. Ganesan, and N. Chilakapati, "Fireworks Enriched P&O Algorithm for GMPPT and Detection of Partial Shading in PV Systems," *IEEE Transactions on Power Electronics,* vol. 32, no. 6, pp. 4432-4443, 2017.
[24] C. Manickam, G. R. Raman, G. P. Raman, S. I. Ganesan, and C. Nagamani, "A Hybrid Algorithm for Tracking of GMPP Based on P&O and PSO With Reduced Power Oscillation in String Inverters," *IEEE Transactions on Industrial Electronics,* vol. 63, no. 10, pp. 6097-6106, 2016.
[25] K. Sundareswaran and S. Palani, "Application of a combined particle swarm optimization and perturb and observe method for MPPT in PV systems under partial shading conditions," *Renewable Energy,* vol. 75, pp. 308-317, 2015.
[26] S. Mohanty, B. Subudhi, and P. K. Ray, "A Grey Wolf-Assisted Perturb & Observe MPPT Algorithm for a PV System," *IEEE Transactions on Energy Conversion,* vol. 32, no. 1, pp. 340-347, 2017.
[27] K. Ishaque, Z. Salam, and H. Taheri, "Simple, fast and accurate two-diode model for photovoltaic modules," *Solar Energy Materials and Solar Cells,* vol. 95, no. 2, pp. 586-594, 2011.
[28] M. G. Villalva and J. R. Gazoli, "Comprehensive approach to modeling and simulation of photovoltaic arrays," *Power Electronics, IEEE Transactions on,* vol. 24, no. 5, pp. 1198-1208, 2009.
[29] J. Ahmed and Z. Salam, "An improved perturb and observe (P&O) maximum power point tracking (MPPT) algorithm for higher efficiency," *Applied Energy,* vol. 150, pp. 97-108, 2015.
[30] J. Ahmed and Z. Salam, "An Accurate Method for MPPT to Detect the Partial Shading Occurrence in a PV System," *IEEE Transactions on Industrial Informatics,* vol. 13, no. 5, pp. 2151- 2161, 2017.
[31] Y.-H. Liu, J.-H. Chen, and J.-W. Huang, "A review of maximum power point tracking techniques for use in partially shaded conditions," *Renewable and Sustainable Energy Reviews,* vol. 41, no. 0, pp. 436-453, 1// 2015.
[32] J. Ahmed and Z. Salam, "An Improved Method to Predict the Position of Maximum Power Point During Partial Shading for PV Arrays," *Industrial Informatics, IEEE Transactions on,* vol. 11, no. 6, pp. 1378-1387, 2015.
[33] K. S. Tey and S. Mekhilef, "Modified incremental conductance algorithm for photovoltaic system under partial shading conditions and load variation," *IEEE Transactions on Industrial Electronics,* vol. 61, no. 10, pp. 5384-5392, 2014.

